J. Fluid Mech. (2024), *vol*. 982, A19, doi:10.1017/jfm.2024.118

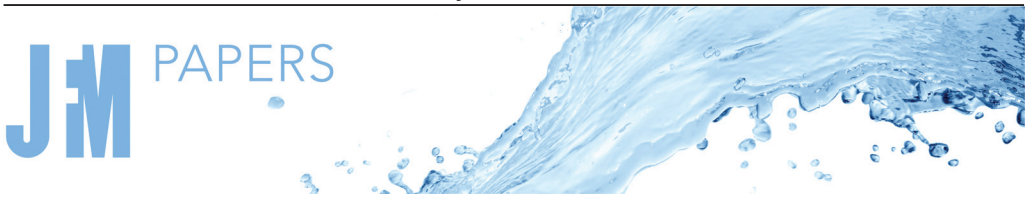

Exploring slip effects of ferrofluid film flow over a slanted rough surface

Anupam Bhandari[1],† **and K.P.S. Parmar**[2]

[1]Department of Mathematics, School of Engineering, University of Petroleum & Energy Studies (UPES), Energy Acres Building, Bidholi, Dehradun 248007, Uttarakhand, India

[2]Department of Physics, School of Engineering, University of Petroleum & Energy Studies (UPES), Energy Acres Building, Bidholi, Dehradun 248007, Uttarakhand, India

(Received 25 June 2023; revised 2 November 2023; accepted 29 January 2024)

We examined the influences of slip parameters on the velocity and thermal characteristics of a ferrofluid film of fixed thickness. The flow is generated on a rough and inclined whirling surface that is positioned in an external magnetic (dipole) field. The similarity transformation reduces the model equations (continuity, momentum, energy and concentration), and the solution of the normalized coupled ordinary differential equations is carried out through the finite element process. The influences of slip effects, Brownian motion, thermophoresis and a heat source on the velocity (radial, tangential and axial), gravity (drainage, induced), temperature profile and concentration profile are determined. The tangential flow and temperature are both decreased by an increase in the velocity slip parameter, whereas drainage, induced, radial and axial flows are increased. Enlarging the thermal slip parameter decreases the temperature. Improving slip parameters (velocity and thermal) also improves the concentration profile. Both Nusselt and Sherwood numbers are found to improve on improving the velocity slip parameter, while they decrease on decreasing the thermal slip parameter. The results and insights from this work could be applied to a wide range of medicinal fields, such as targeted medication therapy and delivery, tissue engineering, etc. as well as different industrial processes including coating, lubrication, heat transfer, etc.

Key words: colloids, thin films, magnetic fluids

1. Introduction

The nano-sized particles of ferrofluid (colloidal suspension) become visible when placed in an external magnetic field, resulting in spikes, patterns and other shapes visible to the naked eye. Additionally, the particles can be manipulated by magnets, producing intriguing

† Email address for correspondence: pankaj.anupam6@gmail.com

© The Author(s), 2024. Published by Cambridge University Press

https://doi.org/10.1017/jfm.2024.118 Published online by Cambridge University Press

motions and shapes. Ferromagnetic materials and a surfactant can be combined to create a ferrofluid, which is then suspended in a liquid such as water, oil or any other solvent. The right physical and magnetic properties can be ensured by adding extra ingredients such as stabilizers and emulsifiers. Sealing, lubrication, film bearing, dampening and cooling are just a few of the many uses it can be put to (Kole & Khandekar 2021). Loudspeaker technology, robotics, aerospace propulsion and electronic components all frequently use it (Bhandari 2023). These fluids have many biomedical uses, such as cell separation, hyperthermia therapy, targeted drug delivery and magnetic resonance imaging (MRI). Additionally, they can be used to boost contrast in imaging, enabling more precise diagnoses (Oehlsen *et al.* 2022). The special characteristics of ferrofluid thin films, such as their ability to maintain shape even when exposed to magnetic fields, can be used to create sensors that measure magnetic fields more precisely (Nair *et al.* 2011). In order to regulate active flow and possibly increase the lift and attack angle, thin-film magnetic liquids can be used. This could be useful in a variety of applications, including improving aircraft performance and developing sensors that can detect and respond to changes in air pressure (Arias 2021).

Wang (2007) investigated three-dimensional thin-film flow over a twirling surface. The author described the velocity profiles of thin films and compared the numerical solution with the swirling flow problem (Cochran 1934). Gul *et al.* (2018) tried to create a more accurate model of thin-film flow for nanoliquids than previously possible by using fractional-order differential equations. Zeeshan *et al.* (2022) examined the influence of unsteadiness on flow behaviour when placed over a rotating inclined surface. Studying the effect of unsteadiness on thin-film flow over rotating inclined surfaces could provide insights into how different parameters affect the flow dynamics and performance. Sheikholeslami, Hatami & Ganji (2015) scrutinized the influence of Brownian and/or thermophoresis phenomena on fluid flow over a similar geometry as described in Gul *et al.* (2018). Acharya (2021) measured the impact of hydrothermal variation on a chemically reactive nanofluid under suction and injection while the fluid was flowing over an inclined rotating disc and obtained the solution to the similarity equation using a special quasi-linearization method. Shah *et al.* (2019) studied the consequences of Hall's effect and radiative–thermal behaviour in similar types of flow domains. Bhandari & Parmar (2023) created a thin liquid film flow model for ferrohydrodynamic flow induced by a tilted revolved sheet when the surface is exposed to a magnet and used finite element modelling to solve the similarity equation. They also concluded that the magnetic dipole could generate a significant decrease or rise in the thermal convection rate depending on the angle of inclination and relative permittivity of the material. Conroy & Matar (2015) investigated ferrofluidic thin layer flow upon a tilted substrate under the intangible effects of a magnetic field together with a nonlinear magnetic sensitivity. They investigated the system's linear and nonlinear stability to assess the influence of magnetism and used the spectral method to obtain a numerical solution. Kim, Bankoff & Miksis (1992) discovered that electric fields can have a negative effect on the durability of thin films, especially when the inclination angle is large. They also found that the stability of film flow is increased when the electric field strength is reduced.

The spreading shape and speed of fluids are significantly influenced by surface tension. Depending on the geometry of the system, surface tension can increase and/or decrease the spreading speed of a fluid, therefore affecting the flow of fluids (Newtonian as well as non-Newtonian) in different ways (Hu & Kieweg 2012). The fourth-grade model was found to be better at predicting the thin-film characteristics than the Newtonian model and it was found that the presence of slip conditions and the fluid's fourth-grade non-Newtonian

https://doi.org/10.1017/jfm.2024.118 Published online by Cambridge University Press

behaviour were significant aspects of the flow (Sajid *et al.* 2008). Yilbas *et al.* (2022) looked into how the hydrophobicity of a rough surface, which is crucial in biomedical, sensing and separation applications, changes when a ferrofluid droplet is added to it. They discovered that the hydrophobicity of the rough surface was increased by the addition of a ferrofluid drop, making it simpler to control liquids deposited on the surface. Film flow over a tilted plane can experience additional body forces due to an electric field. This implies that the behaviour and hydrodynamic stability of the flow can be affected by an electric field (Chattopadhyay, Mukhopadhyay & Barua 2019). Dawar *et al.* (2022) discovered that the bearing of solar irradiation can raise the temperature of both the nanofluid and the rotating surface, affecting the fluid's viscosity and causing it to stick to the surface. This has implications for practical applications involving nanofluids and rotation. The velocity of the fluid over various surfaces can vary. When studying the flow of fluids over a rotating surface, researchers typically use no-slip conditions. When a rough surface is used, the fluid's velocity can deviate from the surface's velocity (Miklavčič & Wang 2004; Turkyilmazoglu 2010; Mustafa 2017; Alqarni *et al.* 2019).

Govindasamy & Bangalore (2023) introduced a porous medium for a thin-film Casson nanofluid flow over a stretched sheet and measured the heat and mass transfer rate of the flow. Gomathy & Kumar (2023) examined the effects of variable conductivity and viscosity on the thin-film flow across an unstable sheet that is permeable and stretches, taking into account the flow zone described in Govindasamy & Bangalore (2023). Gangadhar, Keziya & Kumar (2018) investigated the impact of convective heating and thermal radiation on the temperature of the ferrohydrodynamic flow over a stretching cylinder. Brownian motion and thermophoresis have a significant influence on the temperature distribution in the current situation because ferrofluids are colloidal suspensions of nanoparticles. In colloidal liquids, Michaelides (2015) elucidated the significance of Brownian motion and the thermophoresis of nanoparticles, as well as the interplay between these physical phenomena. In their mathematical model for the convective flow of a nanofluid along a vertical frustum, Motsa, RamReddy & Venkata Rao (2017) examined the effects of thermophoresis and Brownian motion. When examining heat transport in colloidal suspensions, the radiant heat flux is a crucial component. Bryant *et al.* (2003) demonstrated the uncertainties associated with heat flux measurements. When examining heat transport in various fluid types, researchers take into account the influence of thermal radiation (Ummeda & Ontela 2023; Srivastav & RamReddy 2023*a*,*b*). A heat source is a source of high-temperature thermal energy that emits heat without losing heat. Thumma *et al.* (2023) looked at how a rotating surface's hybrid nanofluid flow was affected by the radiative heat flux and heat source parameters. In order to better understand heat transport in fluids, the researchers presented the effects of radiative heat flow, thermophoresis and Brownian motion (Chamkha *et al.* 2014).

The literature review that is currently available illustrates several thin-film flow patterns for various fluid types. Ferrofluid thin-film flow over an inclined rotating surface is not addressed by the literature currently in publication concerning the effects of thermal and velocity slip. The literature shows that no research has yet been done on the thin-film layer flow of a ferrofluid over an oblique and rough spinning surface. Herein, we consider the flow of a ferrofluid thin film on an angled spinning surface with slip effects in a fixed field of a magnetic dipole. The axis of rotation is not parallel to the gravitational force in this instance. The behaviour of the flow as a function of temperature is also considered, as are radiative heat flux and heat source effects. A layer of ferrofluid will have slip effects on the surface due to the roughness factor. This study shows how surface roughness affects velocities, temperature, concentration, stress and heat transfer. The fully

https://doi.org/10.1017/jfm.2024.118 Published online by Cambridge University Press

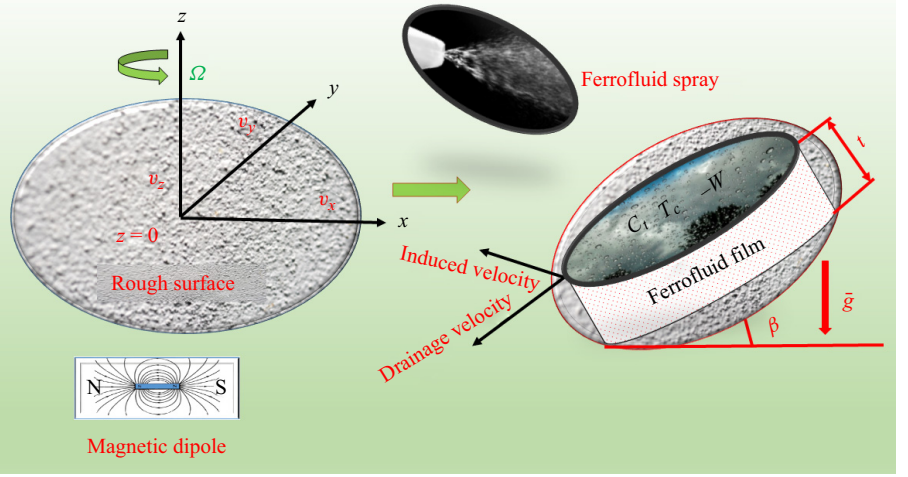

Figure 1. Demonstration of ferrohydrodynamic flow over an inclined rough surface under a magnetic dipole as per the boundary conditions given in (2.8) and (2.9).

developed three-dimensional flow of ferrofluid is studied using the Cartesian form of the Navier–Stokes equations. The end effects can be disregarded because the film thickness is negligible in relation to the disc's radius. Wang's (2007) similarity operation is used to normalize the governing equations (GEs). With this modification, a set of ordinary differential equations (ODEs) is created from the partial differential equations (PDEs). Numerical computations of the normalized differential equations (NDEs) are obtained via the finite element procedure in COMSOL Multiphysics software, and the solution is compared with the earlier numerical results. It would be good to do an experimental confirmation of this fascinating phenomenon.

The flow over an angled and rough rotating surface with slip effects in the presence of dipoles and temperature variations could provide valuable insight into how ferrofluids behave under such conditions. The findings of such a study could have practical applications in a variety of fields. The role of concentration variation in the flow is also considered in this work. Taking concentration variation in the flow into account could provide a better understanding of how ferrofluids behave in this type of environment. It may also aid in finding the most effective conditions for ferrofluid applications. This research could be used to improve biosensors, medical imaging techniques and therapy.

2. Mathematical equations for ferrohydrodynamics

Figure 1 is a representation of ferrohydrodynamic flow due to rotation in an oblique, rough magnetized plane. The whole physical phenomenon is demonstrated in two parts in this figure. In the first part of the figure, we consider a rough disc that rotates with uniform angular velocity. At a fixed distance, the disc is controlled by a magnetic dipole. The velocity components (v_x, v_y, v_z) of the magnetic fluid are considered along the axes x, y and z, respectively. The actual flow of the present study is represented in the second part of the figure. In this case, we consider that the ferrofluid is deposited through a spraying velocity W over an inclined and rough surface. Let the radius of the rough circular disc be large in comparison with the depth (t) of the deposited film. Under slip conditions, flow occurs over the spinning disc, but the gravitational force causes a drainage flow on the slanted surface. However, the flow is induced in the y direction by surface rotation and gravitational forces. The magnitude of gravity $(\bar{g})$ works in the downward direction,

https://doi.org/10.1017/jfm.2024.118 Published online by Cambridge University Press

as shown in the figure. Suppose T_c denotes the Curie temperature and C_t denotes the concentration on the film layer. We use the Cartesian form of coordinates since edge effects are neglected. This assumption presents the three-dimensional flow of ferrofluid film in this domain. However, most of the previous theoretical models of rotating flows were based on two-dimensional axisymmetric flows. The GEs in the three-dimensional Cartesian configuration are given in Wang (2007), Sheikholeslami *et al.* (2015), Bacri *et al.* (1995) and Andersson & Valnes (1998) as

$$\frac{\partial v_x}{\partial x}+\frac{\partial v_y}{\partial y}+\frac{\partial v_z}{\partial z}=0, \tag{2.1}$$

$$v_x\frac{\partial v_x}{\partial x}+v_y\frac{\partial v_x}{\partial y}+v_z\frac{\partial v_x}{\partial z}=\nu\left\{1+\frac{3}{2}\varphi\frac{\xi-\tanh\xi}{\xi+\tanh\xi}\sin^2\vartheta\right\}\left(\frac{\partial^2 v_x}{\partial x^2}+\frac{\partial^2 v_x}{\partial y^2}+\frac{\partial^2 v_x}{\partial z^2}\right)+\bar{g}\sin\beta+\frac{\mu_0}{\rho}M\frac{\partial H}{\partial x}, \tag{2.2}$$

$$v_x\frac{\partial v_y}{\partial x}+v_y\frac{\partial v_y}{\partial y}+v_z\frac{\partial v_y}{\partial z}=\nu\left\{1+\frac{3}{2}\varphi\frac{\xi-\tanh\xi}{\xi+\tanh\xi}\sin^2\vartheta\right\}\left(\frac{\partial^2 v_y}{\partial x^2}+\frac{\partial^2 v_y}{\partial y^2}+\frac{\partial^2 v_y}{\partial z^2}\right), \tag{2.3}$$

$$v_x\frac{\partial v_z}{\partial x}+v_y\frac{\partial v_z}{\partial y}+v_z\frac{\partial v_z}{\partial z}=\nu\left\{1+\frac{3}{2}\varphi\frac{\xi-\tanh\xi}{\xi+\tanh\xi}\sin^2\vartheta\right\}\left(\frac{\partial^2 v_z}{\partial x^2}+\frac{\partial^2 v_z}{\partial y^2}+\frac{\partial^2 v_z}{\partial z^2}\right)-\frac{1}{\rho}\frac{\partial p}{\partial z}-\bar{g}\cos\beta+\frac{\mu_0}{\rho}M\frac{\partial H}{\partial z}, \tag{2.4}$$

$$\begin{aligned}&v_x\frac{\partial T}{\partial x}+v_y\frac{\partial T}{\partial y}+v_z\frac{\partial T}{\partial z}-\frac{\mu_0}{\rho c_p}T\frac{\partial M}{\partial T}\left(v_x\frac{\partial H}{\partial x}+v_y\frac{\partial H}{\partial y}+v_z\frac{\partial H}{\partial z}\right)\\&=\alpha\left(\frac{\partial^2 T}{\partial x^2}+\frac{\partial^2 T}{\partial y^2}+\frac{\partial^2 T}{\partial z^2}\right)+D_B\left\{\frac{\partial C}{\partial x}\frac{\partial T}{\partial x}+\frac{\partial C}{\partial y}\frac{\partial T}{\partial y}+\frac{\partial C}{\partial z}\frac{\partial T}{\partial z}\right\}\\&\quad+\frac{D_T}{T}\left\{\left(\frac{\partial T}{\partial x}\right)^2+\left(\frac{\partial T}{\partial y}\right)^2+\left(\frac{\partial T}{\partial z}\right)^2\right\}-\frac{1}{\rho c_p}\frac{\partial q_r}{\partial z}+\frac{Q}{\rho c_p}(T-T_c),\end{aligned} \tag{2.5}$$

$$\begin{aligned}&v_x\frac{\partial C}{\partial x}+v_y\frac{\partial C}{\partial y}+v_z\frac{\partial C}{\partial z}=D_B\left(\frac{\partial^2 C}{\partial x^2}+\frac{\partial^2 C}{\partial y^2}+\frac{\partial^2 C}{\partial z^2}\right)\\&\qquad+\frac{D_T}{T_0}\left\{\left(\frac{\partial T}{\partial x}\right)^2+\left(\frac{\partial T}{\partial y}\right)^2+\left(\frac{\partial T}{\partial z}\right)^2\right\}.\end{aligned} \tag{2.6}$$

In the GEs, ν indicates the kinematic viscosity, φ implies the volume fraction, ξ implies the Langevin parameter, ϑ signifies the obliqueness between the magnetic field and vorticity, μ_0 signifies the permeability of free space, ρ indicates density, M implies magnetization, H implies magnetic field intensity, α denotes the thermal diffusivity, T denotes the temperature, p denotes the pressure, α stands for the thermal diffusivity, D_B implies the Brownian diffusion coefficient, D_T implies thermophoretic coefficient, c_p implies the specific heat, Q implies the heat source, C implies the concentration variable and T_0 denotes the initial temperature.

https://doi.org/10.1017/jfm.2024.118 Published online by Cambridge University Press

Equation (2.1) is the equation of continuity; (2.2)–(2.4) are the equations of motion. The expression for the energy equation is shown by (2.5), and the concentration equation is represented by (2.6). Except for $(1+\frac{3}{2}\varphi((\xi-\tanh\xi)/(\xi+\tanh\xi))\sin^2\vartheta)$, $(\mu_0/\rho)M(\partial H/\partial x)$ and $(\mu_0/\rho)M(\partial H/\partial z)$, all of the terms in (2.1)–(2.4) are already available in the literature (Wang 2007; Sheikholeslami *et al.* 2015) for ordinary viscous flow. When the vorticity is in line with the field, the expression $\frac{3}{2}\varphi((\xi-\tanh\xi)/(\xi+\tanh\xi))\sin^2\vartheta$ becomes zero, indicating that the magnetic field's effect on viscosity is effectively non-existent. The difference between magnetic and viscous torques causes a rotational viscosity effect.

The term in the energy equation that takes into account the magnetic field, temperature and velocities is a representation of the thermo-mechanical interaction because of the magnetism (Neuringer & Rosensweig 1964). The coefficient D_B in (2.5) and (2.6) is decided by the size of the particles and the properties of fluid and is particularly significant when the particle size is less than 0.1 micrometres. This is a crucial consideration when dealing with ferrofluids, as the nanoparticles they are composed of create additional complexities. The thermo-diffusion coefficient, temperature gradient and radiative heat flux play important roles in the energy equation for research involving ferrofluids. The parameter D_T in the energy equation is the thermo-diffusion coefficient, which is the ratio of the thermophoretic velocity to the temperature gradient. Additionally, the variable q_r denotes the radiative heat flux, which follows the Stefan–Boltzmann radiative law and can lead to nonlinear radiation effects (Steward & Cannon 1971; Mahanthesh 2021). Mathematically, this can be evaluated as follows:

$$q_r = -\frac{4\sigma^*}{3k^*}\frac{\partial T^4}{\partial z} = -\frac{16\sigma^*}{3k^*}T^3\frac{\partial T}{\partial z}. \tag{2.7}$$

In (2.7), σ^* stands for the Stefan–Boltzmann constant and k^* implies the average absorption coefficient.

2.1. *Slip effects of inclined rotating surfaces with roughness*

In most cases, it is difficult to achieve a perfectly smooth surface due to the natural imperfections or irregularities that occur on most surfaces. For this reason, a perfectly smooth surface is often hard to attain (Miklavčič & Wang 2004). We use slip conditions with a slip length parameter L_1 in the boundary conditions to accurately model the surface. This parameter specifies how much liquid is allowed to pass through the surface (Turkyilmazoglu 2010). This slip length parameter measures the length beyond which the liquid velocity linearly extrapolates to zero (Wang *et al.* 2021). The initial and boundary conditions with slip effects are as follows (Mustafa 2017; Alqarni *et al.* 2019):

$$\text{At } z=0, \quad \begin{cases} v_x = -\Omega y + L_1\dfrac{\partial v_x}{\partial z} \\ v_y = \Omega x + L_1\dfrac{\partial v_y}{\partial z} \\ v_z = 0 \\ T = T_0 + L_2\dfrac{\partial T}{\partial z} \\ D_B\dfrac{\partial C}{\partial z} + \dfrac{D_T}{T_c}\dfrac{\partial T}{\partial z} = 0 \end{cases}, \tag{2.8}$$

https://doi.org/10.1017/jfm.2024.118 Published online by Cambridge University Press

$$\text{At } z = t, \quad \begin{cases} \dfrac{\partial v_x}{\partial z} = 0 \\ \dfrac{\partial v_y}{\partial z} = 0 \\ v_z = -W \\ T = T_c \\ C = C_t \\ p = P_t \end{cases} . \tag{2.9}$$

In the above equations, the expressions $L_1(\partial v_x/\partial z)$ and $L_1(\partial v_y/\partial z)$ represent the slip velocities in the radial and tangential regions of the surface, where L_1 denotes the slip length which is related to the viscosity of the ferrofluid and the interfacial friction (Nicholson *et al.* 2019). The expression $L_2(\partial T/\partial z)$ represents the thermal slip due to a rough surface. Thermal slip in fluid flow is a phenomenon in which the fluid velocity is greater near the boundary of a hot surface than it is further away. This is the result of fluid particles' interactions with the temperature gradient, which cause an imbalance in the momentum of particles near the hot surface compared with those further away. The parameter L_2 represents the temperature jump. Based on the wettability of the surface, the slip length can be either positive (+ive) or negative (−ive). These slip conditions, however, are considered for a water-based ferrofluid. As a result, slip parameters can be described using either hydrophobic or hydrophilic surfaces. The temperature jump in ferrofluids could be useful for heat transfer applications and electronic device cooling. Temperature shielding can be accomplished by using large temperature jumps. It can be used to control the heat in electronic devices as well as in medical applications that require localized heating. The parameter P_t denotes the pressure on the film.

2.2. *Exploring the magnetic effect and the equation of state*

In the current problem, the dipole is placed at the centre (middle) of the z-axis; however, it is fixed at a distance (a) below the z-axis. The applied magnetic field $\boldsymbol{H} = H_x\hat{i} + H_y\hat{j} + H_z\hat{k}$ is equal to the scalar potential function's negative gradient ($-\nabla A$), where H_x, H_y and H_z denote the strength of the magnetic field in the x-axis (radial), y-axis (tangential) and z-axis (axial) directions, respectively, and, $\hat{i}$, $\hat{j}$ and $\hat{k}$ represent the corresponding unit vectors. We write it mathematically as $\boldsymbol{H} = -\nabla A$. The magnetic scalar potential function caused by the magnetic dipole is (Rosensweig 1985)

$$A = \frac{\gamma_0}{2\pi}\frac{x}{x^2 + (z+a)^2}, \tag{2.10}$$

where γ_0 represents the dipole moment per unit length. Using (2.10), the component-wise magnetic field intensity can be calculated as (Andersson & Valnes 1998)

$$\frac{\partial H}{\partial x} = -\frac{\partial A}{\partial x} = \frac{\gamma_0}{2\pi}\frac{x^2 - (z+a)^2}{[x^2 + (z+a)^2]^2}, \quad \frac{\partial H}{\partial y} = 0, \quad \frac{\partial H}{\partial z} = -\frac{\partial A}{\partial z} = \frac{\gamma_0}{2\pi}\frac{2x(z+a)}{[x^2 + (z+a)^2]^2}. \tag{2.11a–c}$$

https://doi.org/10.1017/jfm.2024.118 Published online by Cambridge University Press

The magnetic body force due to magnetic dipole is $\mu_0 M \nabla H$ and the resultant determinable magnetic strength (Andersson & Valnes 1998)

$$H = [(H_x)^2 + (H_y)^2 + (H_z)^2]^{1/2}. \tag{2.12}$$

Using (2.11*a–c*) and (2.12), we can compute the parts of the magnetic field gradient (Neuringer 1966). Thereafter, these expressions can be used in the momentum equations (2.2) and (2.4). These components are

$$\frac{\partial H}{\partial x} = \frac{\dfrac{\partial A}{\partial x}\dfrac{\partial^2 A}{\partial x^2} + \dfrac{\partial A}{\partial z}\dfrac{\partial^2 A}{\partial x\,\partial z}}{\left[\left(\dfrac{\partial A}{\partial x}\right)^2 + \left(\dfrac{\partial A}{\partial z}\right)^2\right]^{1/2}}, \quad \frac{\partial H}{\partial z} = \frac{\dfrac{\partial A}{\partial x}\dfrac{\partial^2 A}{\partial x\,\partial z} + \dfrac{\partial A}{\partial z}\dfrac{\partial^2 A}{\partial z^2}}{\left[\left(\dfrac{\partial A}{\partial x}\right)^2 + \left(\dfrac{\partial A}{\partial z}\right)^2\right]^{1/2}}. \tag{2.13a,b}$$

The component of the gradient in the y direction $\partial H/\partial y$ becomes automatically zero because the scalar potential function is considered to be composed of two variables x and z. We consider the second-order approximation of the variable x. This approximation reduces the components of the magnetic field gradient as (Andersson & Valnes 1998)

$$\frac{\partial H}{\partial x} = -\frac{\gamma_0}{2\pi}\frac{2x}{(z+a)^4}, \quad \frac{\partial H}{\partial z} = \frac{\gamma_0}{2\pi}\left[-\frac{2}{(z+a)^3} + \frac{4x^2}{(z+a)^5}\right]. \tag{2.14a,b}$$

Temperature shifts influence the magnetic force of ferrofluid, and temperature variations can alter ferrofluid magnetism (Zablotsky, Mezulis & Blums 2009). At average temperature T_a the magnetic field H_0 follows an equation of state, or the equilibrium state at temperature T_a is determined by the equation of state for H_0 as Finlayson (1970), Zebib (1996)

$$M = M_0 + \left(\frac{\partial M}{\partial H}\right)_{H_0,T_a}(H - H_0) + \left(\frac{\partial M}{\partial T}\right)_{H_0,T_a}(T - T_a). \tag{2.15}$$

When the magnetism is sufficient to saturate the ferrofluid within the boundary layer, it could be described by an equation (linear) of the state between the extreme temperatures experienced by the fluid (Neuringer 1966). The approximation of the linear equation of state is (Neuringer & Rosensweig 1964)

$$M = -\left|\frac{\partial M}{\partial T}\right|(T - T_c), \tag{2.16}$$

where $|\partial M/\partial T| = K$ represents the pyro-magnetic coefficient and T_c implies the Curie temperature.

3. Normalizing the thin-film flow equations

The PDEs concerning ferrohydrodynamic thin-film flow can be simplified into a set of nonlinear ODEs. Wang (2007) suggested the following similarity transformation:

$$\left.\begin{gathered} v_x = -\Omega y g(\eta) + \Omega x f'(\eta) + \frac{\bar{g}\sin\beta h(\eta)}{\Omega}, \quad v_y = \Omega x g(\eta) + \Omega y f'(\eta) + \frac{\bar{g}\sin\beta k(\eta)}{\Omega}, \\ v_z = -2\sqrt{\Omega\nu}\, f(\eta), \quad T = T_c - T_1(\eta)(T_c - T_0), \quad C = C_t + C_1(\eta)(C_0 - C_t), \\ \eta = z\left(\frac{\Omega}{\nu}\right)^{1/2}, \quad \zeta = x\left(\frac{c\rho}{\mu}\right)^{1/2}. \end{gathered}\right\} \tag{3.1}$$

https://doi.org/10.1017/jfm.2024.118 Published online by Cambridge University Press

By satisfying (2.1) and degenerating (2.2)–(2.6) and (2.8) and (2.9), this transformation produces a set of nonlinear coupled differential equations:

$$Rf''' + 2ff'' - (f')^2 + g^2 = 0, \tag{3.2}$$

$$Rg'' - 2gf' + 2fg' = 0, \tag{3.3}$$

$$Rh'' - hf' + kg + 2fh' - F_m \frac{\zeta}{(\eta + \alpha_1)^4}\theta + 1 = 0, \tag{3.4}$$

$$Rk'' + 2fk' - kf' - hg = 0, \tag{3.5}$$

$$\begin{aligned}\frac{1}{Pr}\left[T_1''\left\{1 + \frac{4}{3}N(1 + T_1(T_R - 1))^3\right\} + \frac{4}{3}N\{3(1 + T_1(T_R - 1))^2(T_R - 1)(T_1')^2\}\right] \\ + 2fT_1' + NbC_1'T_1' + Nt(T_1')^2 + \lambda T_1 + F_1\frac{\zeta}{(\eta + \alpha_1)^4}(T_1 - \varepsilon)h \\ - F_2(\theta - \varepsilon)f\left[\frac{2}{(\eta + \alpha_1)^3} - \frac{4\zeta^2}{(\eta + \alpha_1)^5}\right] = 0,\end{aligned} \tag{3.6}$$

$$C_1'' + \frac{Nt}{Nb}T_1'' + ScfC_1' = 0. \tag{3.7}$$

In (3.2)–(3.7), the parameter $R = 1 + \frac{3}{2}\varphi\xi((\xi - \tanh\xi)/(\xi + \tanh\xi))\sin^2\alpha_m$ represents the rotational viscosity parameter. This parameter depends on the parameter ξ, which is the index of magnetic energy (and thermal energy) and the volume fraction (φ) of the magnetic particles. However, if the field is parallel to the vorticity, then this parameter becomes zero. The parameter $F_m = \mu_0 K\gamma_0(T_c - T_w)\Omega^2/\pi\bar{g}\ \rho c^{1/2}\nu^{3/2}\sin\beta$ represents the influence of the magnetization force on the flow. The parameter $\alpha_1 = a(\Omega/\nu)^{1/2}$ represents the effect of the distance of the dipole from the surface of the plate. The parameter $Pr = \nu/\alpha$ represents the Prandtl number and it is a dimensionless number used to express the proportion between thermal diffusivity and momentum diffusivity. The parameter $N = 4\sigma^* T_c^3/3k^*k$ denotes the radiation parameter and it describes the rate of radiation-based heat transfer in a homogeneous medium and is a function of the temperature, absorption coefficient and the Stefan–Boltzmann constant. The parameter $T_R = T_0/T_c$ denotes the temperature ratio parameter. The parameters $F_1 = \mu_0 K\gamma_0\bar{g}\sin\beta\Omega^2/2\pi\ c_p\rho c^{1/2}\nu^{3/2}$ and $F_2 = \mu_0 K\gamma_0\Omega/2\pi c_p\rho\nu$ represent the ferromagnetic interaction numbers and they measure the relative strengths of ferromagnetic interactions between particles and fluid. The parameter $\varepsilon = T_c/(T_c - T_0)$ denotes the dimensionless Curie temperature and it is used to describe the temperature at which a material undergoes a phase change from one magnetic state to another. The strength of the Brownian motion in comparison with other fluid motions is expressed by the Brownian motion parameter $Nb = D_B(C_0 - C_t)/\nu$. The relative strength of thermophoretic forces in a fluid is measured using the thermophoresis parameter $Nt = D_T(T_c - T_0)/\nu T_c$. The strength of the heat source or sink in relation to the fluid's actual thermal diffusivity is described by the heat source/sink parameter $\lambda = Q/\Omega\rho c_p$. How well different molecules transfer heat and momentum in a laminar flow is determined by the Schmidt number Sc.

https://doi.org/10.1017/jfm.2024.118 Published online by Cambridge University Press

The similarity transformation simplifies the initial and boundary conditions by transforming them into a normalized form

$$\left.\begin{array}{c} f(0)=0, \quad f'(0)=\gamma f''(0), \quad g(0)=1+\gamma g'(0), \quad h(0)=\gamma h'(0) \\ k(0)=\gamma k'(0), \quad T_1(0)=1+\alpha T_1'(0), \quad C_1'(0)-\dfrac{Nt}{Nb}T_1'(0)=0 \end{array}\right\}, \tag{3.8}$$

$$f''(\delta)=0, \quad g'(\delta)=0, \quad h'(\delta)=0, \quad k'(\delta)=0, \quad T_1(\delta)=0, \quad C_1(\delta)=0 \text{ at } \eta=\delta. \tag{3.9}$$

The parameters $\gamma = L_1(\Omega/\nu)^{1/2}$ and $\gamma_1 = L_2(\Omega/\nu)^{1/2}$ in the equations above stand for the velocity slip parameter and thermal slip parameter, respectively. The symbol denotes the normalized and constant film thickness δ. Utilizing the equation below, it can be calculated

$$\delta = t(\Omega/\nu)^{1/2}. \tag{3.10}$$

3.1. *Local heat transfer and mass transport quantity*

The speed at which heat moves from the surface of a slanted plate to a thin film is known as the local rate of heat transfer. The rate of convective heat transfer between two surfaces in a flow is determined using the dimensionless Nusselt number (Nu). The quantity is calculated by dividing the convective heat transfer by the conductive heat transfer

$$Nu = \frac{t[-\kappa(T_z)_{z=0}+(q_r)_{z=0}]}{\kappa(T_c-T_w)} = -\left[1+\frac{4N}{3}\{1+(T_R-1)T_1(0)\}^3\right]\delta T_1'(0). \tag{3.11}$$

The ratio of diffusive mass flux to convective mass flux determines the mass transport quantity. The Sherwood number (Sh) is a dimensionless number that is used to calculate the mass transport rate in a particular flow system

$$Sh = \frac{-tC_z}{(C_w-C_0)} = -\delta C_1'(0). \tag{3.12}$$

4. Analysis and convergence of numerical solutions

We employ the finite element technique in the COMSOL Multiphysics program to numerically compute (3.2)–(3.7) and the boundary conditions are given in (3.8) and (3.9) numerically. We set the relative tolerance to 0.0000001. When solving a system of equations, the relative tolerance determines the extent of convergence. It is defined as the ratio of the absolute and relative errors and is set to a specific value before solving. When the relative error exceeds the tolerance, the solver will stop and report an error. The convergence plot can be seen in figure 2 for the results of the normalized equations of the system. The convergence plot in COMSOL Multiphysics is a graphical representation of the solution's progress toward convergence. It displays the residual errors (in blue) as the number of iterations increases. The plot's lines should bend downward, indicating that the errors are decreasing over time. This shows that the solution is approaching a valid result.

During the numerical solution, we take the largest length of the element as 0.0001, the highest element enlargement scale as 1.1 and the resolution of a narrow region as 1. The largest size an element can be before the mesh becomes too coarse is referred to as the maximum element size. This value should be set so that the mesh has enough resolution to capture the solutions but is not too fine, as this can cause the mesh to become too large and slow down the solution process. When optimizing the mesh size and distribution,

https://doi.org/10.1017/jfm.2024.118 Published online by Cambridge University Press

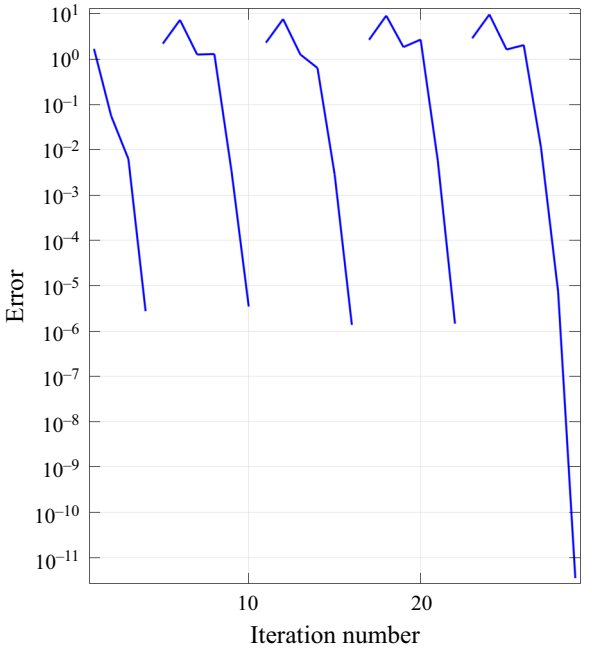

Figure 2. Convergence of numerical solutions using finite element procedures.

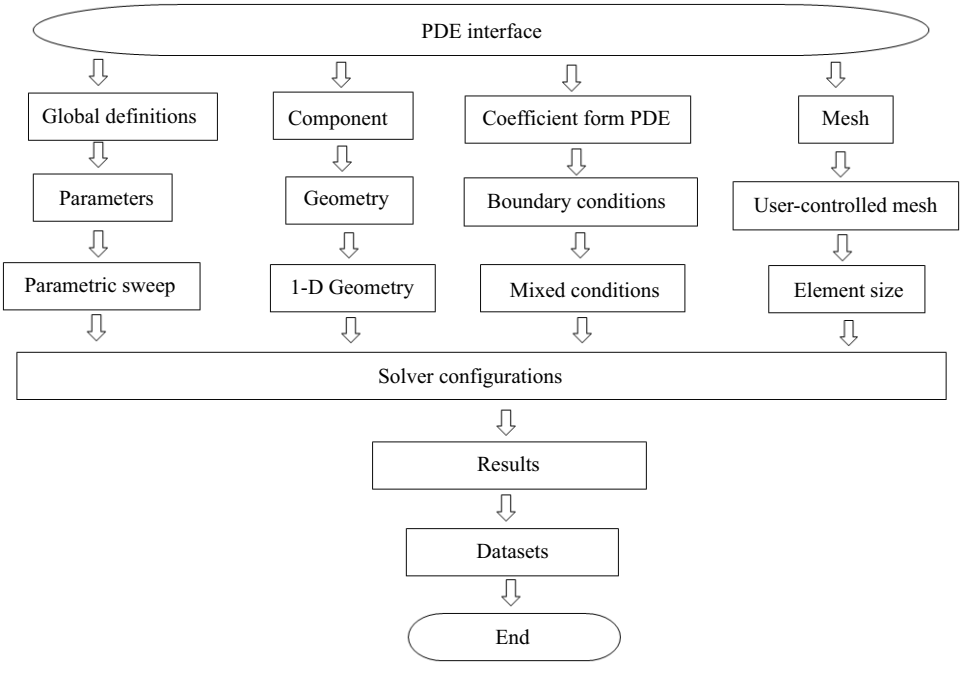

Figure 3. Solution procedure for the NDEs in COMSOL Multiphysics software.

the maximum element growth rate is an important parameter to adjust because it allows the user to control the maximum size of elements while ensuring that the mesh does not become too coarse. The procedure for utilizing COMSOL Multiphysics software to numerically solve the NDE is shown in figure 3.

https://doi.org/10.1017/jfm.2024.118 Published online by Cambridge University Press

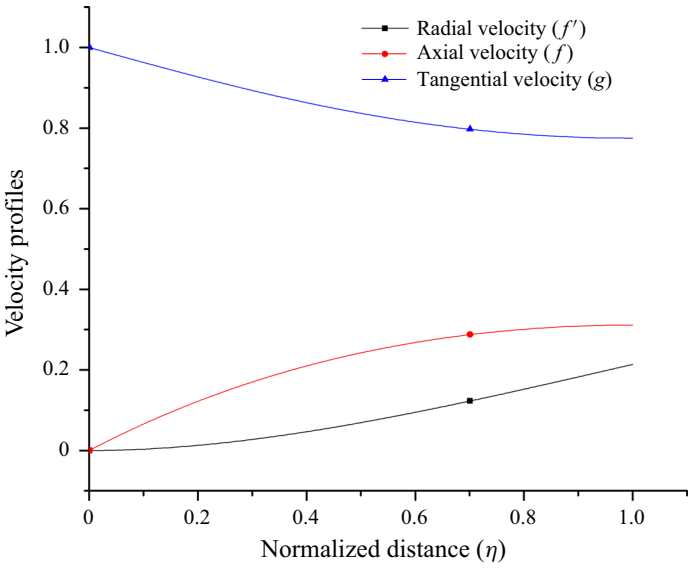

Figure 4. Validation for velocity profiles through finite element procedure exactly matches with Wang's solution (Wang 2007).

4.1. *Validation of solution*

The NDEs reduce to the previous theoretical model by excluding the terms containing Nb and Nt and considering the values of the parameters $R = 0$, $F_m = 0$, $N = 0$, $F_1 = 0$, $F_2 = 0$, $\lambda = 0$. In this case, with no-slip effects, our results for the radial (linear) velocity f', the tangential (angular) velocity g, the axial (vertical) velocity f and the fluid temperature (T_1) profile are in agreement with Wang's numerical solution (Wang 2007). Figure 4 shows the profiles of the axial, radial and tangential velocities, respectively. These results illustrate the special case of the current model, in which the normalized unitless equations are in the form of Wang's normalized case. The findings support the earlier numerical findings (Wang 2007). Figure 5 displays the temperature profile for varied values of the Prandtl number, which are adopted from the previous results (Wang 2007) for comparison. The temperature profile has excellent correspondence to the past solution (Wang 2007). Omitting the abovementioned parameters along with the inclination, the current problem can be simplified to the Kármán swirling problem (Miklavčič & Wang 2004; Turkyilmazoglu 2010). In our case, $f''(0)$ and $g'(0)$ are 0.5102134911 and -0.6159097466, respectively. These values match with the solution of the Kármán swirling flow problem obtained by researchers (Benton 1966; Miklavčič & Wang 2004; Turkyilmazoglu 2010).

5. Description and analysis of results

This manuscript describes the influence of magnetism on the ferrohydrodynamics upon a slanted rotating surface under an applied field of a dipole. The earlier section presents the validation of the present numerical solution. However, in this work, the constant parameters in the solution are the volume fraction (φ) $= 0.05$, magnetic torque-induced parameter (ξ) $= 1$, ferromagnetic interaction number due to a magnetic dipole in the momentum equation (F_m) $= 0.5$, ferromagnetic interaction numbers due to magnetic energy (F_1, F_2) $= 0.5, 0.5$, dimensionless Curie temperature(ε) $= 2$, the distance of

https://doi.org/10.1017/jfm.2024.118 Published online by Cambridge University Press

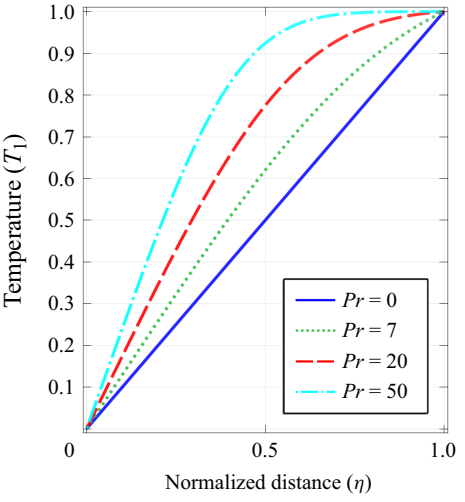

Figure 5. Validation for temperature profile through finite element procedure exactly matches with Wang's solution (Wang 2007).

the dipole from the surface of the plate $(\alpha_1) = 1$, normalized radial distance $(\zeta) = 0.1$, Prandtl number for a water-based ferrofluid $(Pr) = 7$, velocity slip parameter due to a rough surface $(\gamma) = 0.1$, thermal slip parameter $(\gamma_1) = 0.1$, Brownian motion parameter$(Nb) = 0.4$, thermophoresis parameter $(Nt) = 0.1$, heat source parameter $(\lambda) = 0.2$, Schmidt number $(Sc) = 0.08$, radiation parameter $(N) = 0.5$ and temperature ratio parameter $T_R = 1.5$. From previously published literature (Cowley 1989; Blūms, Cebers & Maĭorov 1997; Wang 2007; Acharya 2021; Bhandari 2022), these parameter values are taken into account. However, in the previous study of the flow over an inclined rotating surface, the researchers have considered the large range of Schmidt numbers for which the flow becomes turbulent (Sheikholeslami *et al.* 2015; Acharya 2021). However, the equations consider the laminar flow dynamics.

Figures 6(*a*)–6(*c*) represent the velocity profiles to measure the influence of the coefficient of velocity slippage (γ) on the ferrofluid thin film. The speed at which the fluid is rotating around the centre diminishes when the slip velocity parameter is increased. Because more particles move away from the centre, the radial velocity increases. At the same time, because of the slower rotational speed, the tangential velocity decreases. Axial velocity increases in rotational flow after increasing the slip velocity parameter because, as the slip velocity increases, the flow becomes more intense, causing the axial velocity to increase. This is due to momentum conservation, as increased fluctuation causes the axial velocity to increase while the total flow rate remains constant. Figures 7(*a*) and 7(*b*) show the drainage velocity in the linear direction due to inclination and induced velocity in the angular region due to nonlinearities. The draining velocity of an inclined surface is the speed at which liquid flows down the inclined surface due to gravity. The draining velocity is determined by the surface slope, liquid viscosity and gravitational acceleration. Escalating γ causes a higher gradient in the velocity distribution, which increases the draining velocity. This occurs because a higher slip velocity causes more fluid motion, which increases the force exerted on the liquid due to pressure gradients. This compressive stress gradient causes a faster draining velocity. The Coriolis force, which acts on a moving object and is vertical to the motion of fluid, causes an induced stream in the y direction due to a rotating inclined surface. The speed of the surface's rotation and the angle of

https://doi.org/10.1017/jfm.2024.118 Published online by Cambridge University Press

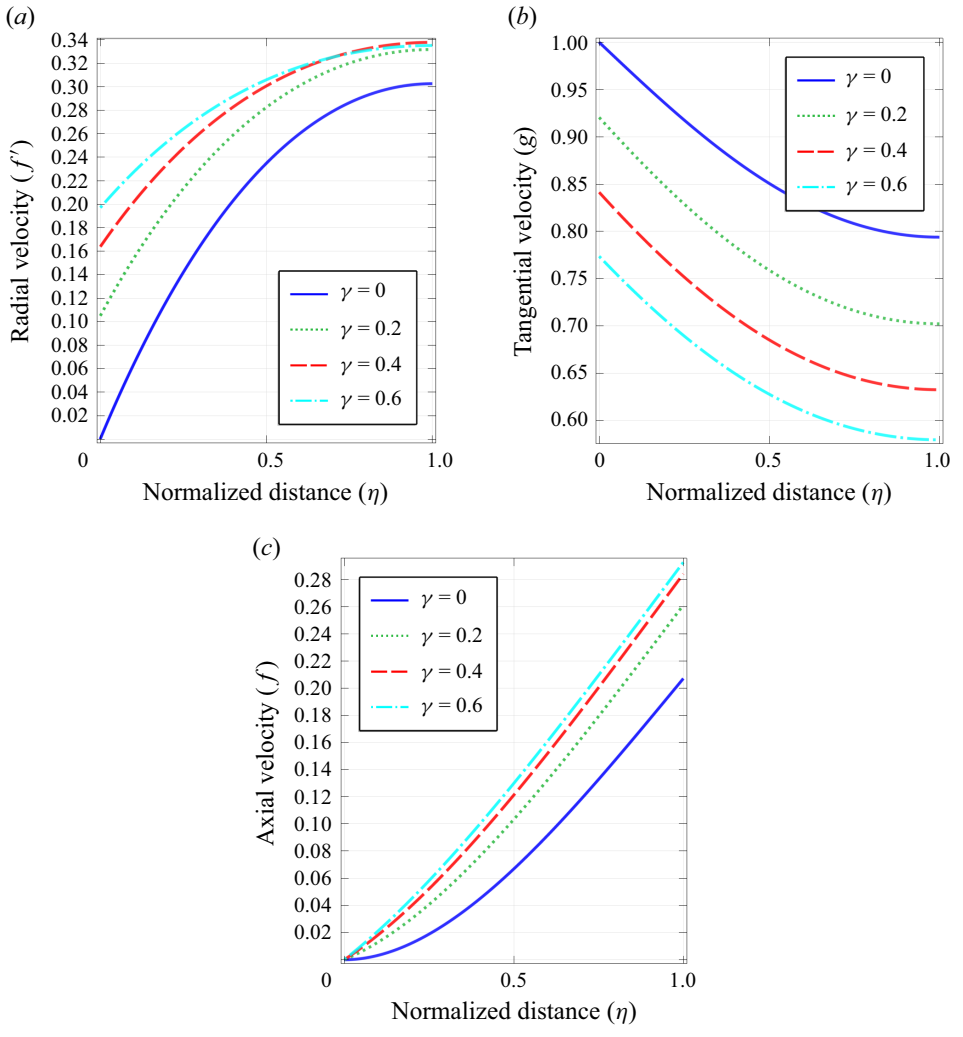

Figure 6. Role of the slip factor γ in the velocity profiles due to inclined flow of ferrofluid thin film.

inclination both affect the amount of flow that is induced as the surface rotates in the y direction. More flow fluctuation from increased velocity slip leads to an imbalance in the stress at the surface. This increased stress causes a greater force on the liquid particles, pushing them along the line of the flow, resulting in a higher induced flow velocity.

Figures 8(a) and 8(b) show the behaviour of temperature and concentration for different ranges of γ. Because of the increased fluid velocity, escalating γ can cause the temperature to drop. The turbulent flow raises the kinetic energy of the fluid particles, which results in a drop in the fluid's internal energy and a lowering of its temperature. Because of the increased fluid velocity, increasing the velocity slip parameter can increase the concentration of the ferrofluid. The increased fluctuation causes more particle mixing, resulting in a higher concentration of ferrofluid. Furthermore, the increased kinetic energy of the particles aids in the breakdown of larger particle clusters, increasing the particle concentration. Figures 9(a) and 9(b) depict how the temperature and concentration of a ferrofluid thin liquid film are affected by the thermal slip parameter (γ_1). The thermal slip

https://doi.org/10.1017/jfm.2024.118 Published online by Cambridge University Press

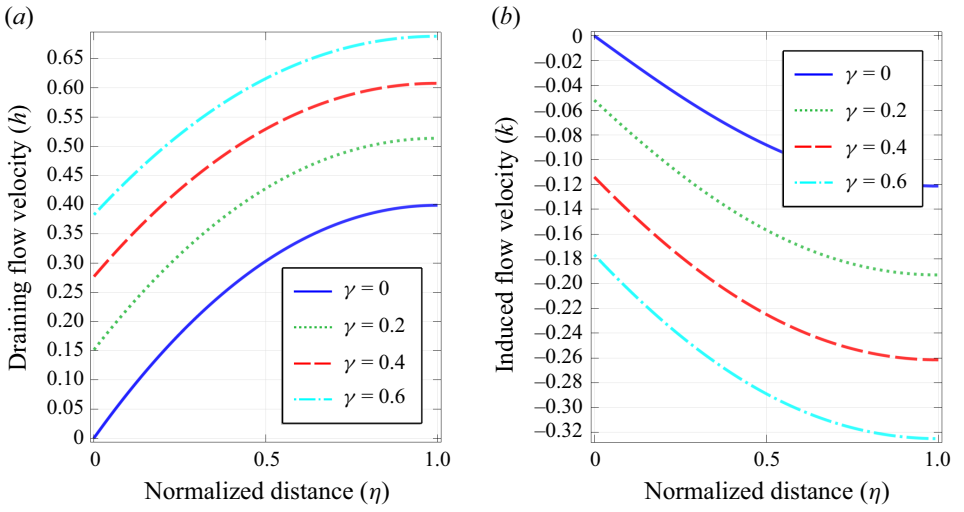

Figure 7. Role of the slip factor in the drainage flow velocity and induced flow velocity of ferrofluid thin film.

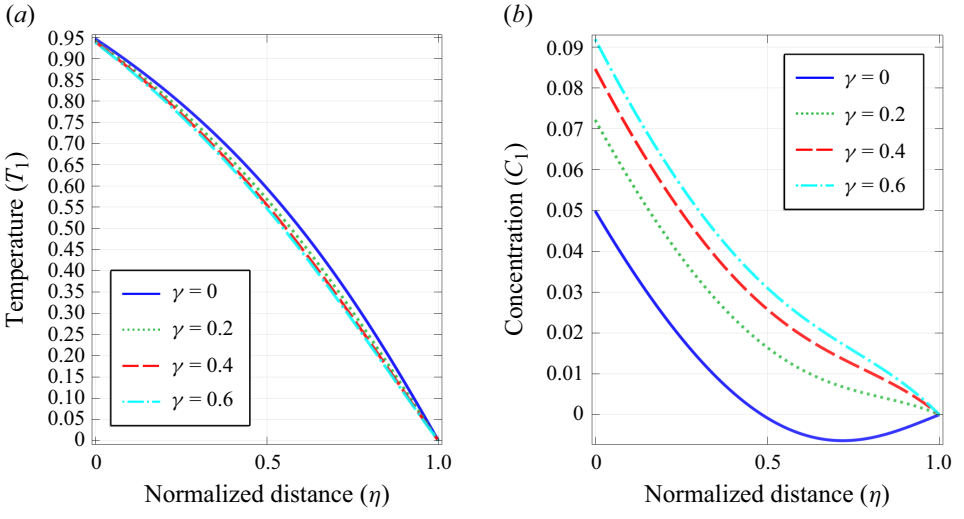

Figure 8. Role of the slip factor in the temperature flow and concentration profile.

parameter measures the thermal difference between the wall and the liquid. The localized temperature gradient at the wall divided by the overall temperature gradient of the bulk fluid yields the thermal slip parameter. It is employed to compute the impact of frictional heating, brought on by the fluid's viscosity, on the wall's temperature. Increasing γ_1 can lower the temperature by diminishing thermal energy transfer from the wall to the fluid. This is because the temperature gradient between the fluid and the wall has decreased, so has the overall rate of heat transfer. Additionally, the increased viscous heating brought on by the elevated thermal slip parameter may help to further lower the wall's temperature, lowering the system's overall temperature. Increasing γ_1 reduces wall-to-fluid thermal energy transfer, lowering the bulk temperature and raising ferrofluid concentration. This aids in producing an environment that is more favourable to particle cluster formation, which ultimately leads to higher concentration. Furthermore, the larger particle clusters

https://doi.org/10.1017/jfm.2024.118 Published online by Cambridge University Press

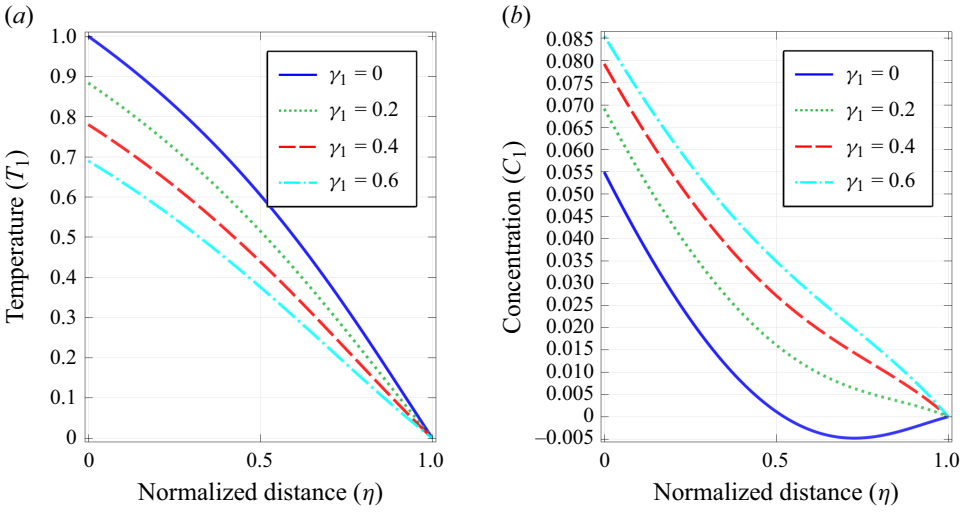

Figure 9. Role of the thermal slip factor in the temperature and concentration profiles.

can be broken up even more by the increased thermal slip parameter. It rises with particle concentration due to the increased viscous heating caused by the increased thermal slip parameter.

Figure 10(*a*) illustrates how the concentration profile is affected by the Brownian motion parameter (*Nb*). The concentration flow decreases as this parameter's value rises. By raising *Nb*, one can reduce the concentration in the flow over a rotating surface because it decreases the particle diffusion rate. This indicates that the particles are moving more slowly, which lowers the concentration overall. More Brownian motion can also make particles more evenly distributed, resulting in lower concentrations in particular flow regions. Figures 10(*b*) and 10(*c*) display the temperature profile as well as the concentration profile for different values of the thermophoresis parameter (*Nt*). This expedites the wall to fluid heat transfer. This is due to a greater temperature difference between the wall and the liquid, which enhances the overall rate of heat transfer. Furthermore, increased thermophoresis can cause particles to become more evenly distributed, resulting in a faster heat transfer rate in specific regions of the flow. Because it increases the rate of particle diffusion, the thermophoresis parameter (*Nt*) increases the concentration near the surface and diminishes it beyond the surface in the stream triggered by a slanted rotating plate. The increased thermal gradient between the wall and the fluid contributes to a faster overall particle diffusion rate. As a result, particles near the wall are more likely to diffuse away from it, causing the concentration near the surface to rise. Particles far from the wall, on the other hand, are more likely to be drawn towards it, resulting in a decrease in concentration far from the surface.

Figures 11(*a*) and 11(*b*) illustrate how the temperature and concentration profile are affected by the heat source parameter (λ). Because it accelerates the rate of heat transfer from the wall to the fluid, the heat source parameter(λ) raises the temperature in the fluid film over an angled spinning surface. Furthermore, the increased heat source can cause the particles to become more evenly distributed, resulting in a higher heat flux rate in a ferrofluid film flow. This variable accelerates the transfer of heat from the surface to the film. As an outcome of the particle's decreased solubility, the temperature of the fluid rises, resulting in a decrease in concentration. Furthermore, the increased heat source can

https://doi.org/10.1017/jfm.2024.118 Published online by Cambridge University Press

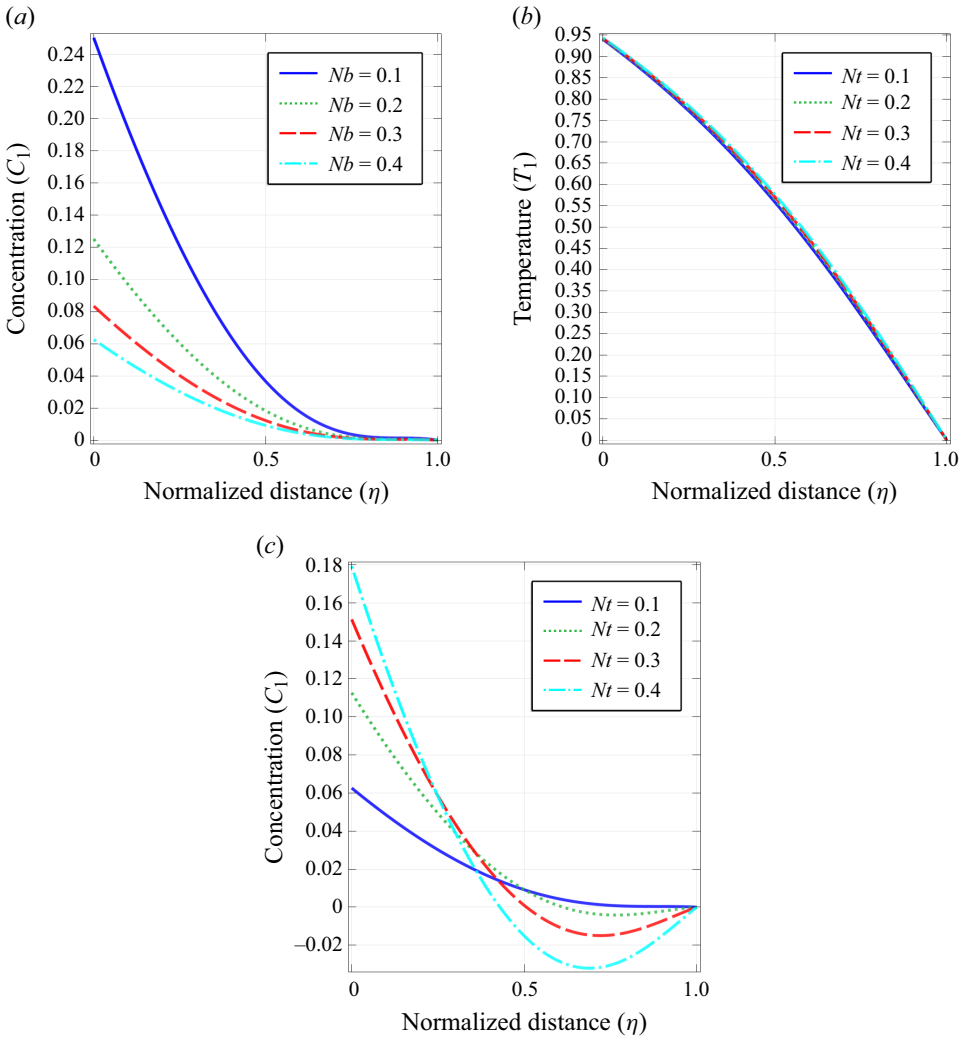

Figure 10. Role of the Brownian motion parameter in the concentration profile and role of the thermophoresis parameter in the temperature and concentration profiles.

cause the particles to become more evenly distributed, resulting in lower concentrations in specific regions of the flow.

Table 1 shows how the Nusselt number (Nu) and Sherwood number (Sh) are affected by γ, γ_1, Nb, Nt and λ. Increasing the velocity slip parameter in an inclined narrow film passing over a spinning surface raises the Nusselt number by lowering the velocity gradient and thus increasing the shear rate and convective heat transfer rate. The Nusselt number consequently increases. Increasing the velocity slip parameter in a fluid flow raises the Sherwood number because it reduces the viscous drag between the two surfaces and makes diffusive mass transfer less dominant, resulting in a higher mass transport rate. Increasing the thermal slip parameter reduces Nu and Sh in the fluid flow because it reduces the temperature gradient between wall and fluid and thus the rate of convective heat transfer and diffusive mass transfer. Consequently, the mass transport rate is reduced, as are the Nusselt and Sherwood numbers. A similar conclusion can be reached for the

https://doi.org/10.1017/jfm.2024.118 Published online by Cambridge University Press

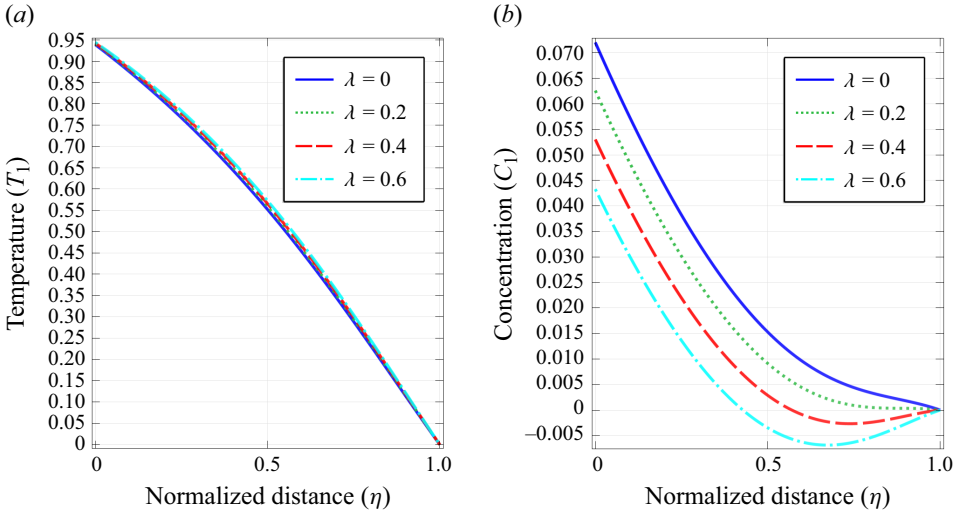

Figure 11. Role of the heat source parameter in the temperature and concentration profiles.

$\boldsymbol{\gamma}$	**0**	**0.2**	**0.4**	**0.6**
Nu	1.784946	1.913060	1.984616	2.026253
Sh	0.142847	0.153555	0.159564	0.1630706
$\boldsymbol{\gamma}_1$	**0**	**0.2**	**0.4**	**0.6**
Nu	1.983447	1.741633	1.532952	1.354954
Sh	0.152572	0.145202	0.137312	0.129191
Nt	**0.1**	**0.2**	**0.3**	**04**
Nu	1.858274	1.822443	1.788464	1.756177
Sh	0.148968	0.291949	0.429421	0.561806
$\boldsymbol{\lambda}$	**0**	**0.2**	**0.4**	**0.6**
Nu	1.912182	1.858274	1.803374	1.747450
Sh	0.153481	0.148968	0.144383	0.139725
Nb	**0.1**	**0.2**	**0.3**	**0.4**
Sh	0.595873	0.297936	0.198624	0.148968

Table 1. Nusselt numbers and Sherwood numbers for different values of the parameters of thermal slip, Brownian motion, thermophoresis and velocity slip.

other parameters listed in table 1. The surface stress in the x and y directions is represented by $h'(0)$ and $k'(0)$, respectively, in the normalized form. Due to a magnetic dipole, it is displayed in table 2 for various values of the velocity slip parameter (γ) and ferromagnetic interaction number (F_m). Stress in the x direction is reduced and stress in the y direction is increased by the velocity slip parameter. On the other hand, stress on the thin film's surface decreases as the ferromagnetic interaction number increases.

6. Outcomes

In the current work, we examined the effects of temperature and velocity slip on ferrofluid thin-film flow across an inclined, rough–rotating surface when a magnetic dipole

https://doi.org/10.1017/jfm.2024.118 Published online by Cambridge University Press

γ	**0**	**0.2**	**0.4**	**0.6**
$h'(0)$	0.824630	0.755735	0.691306	0.637269
$-k'(0)$	0.201619	0.259532	0.284868	0.294516
F_m	**0.5**	**1**	**2**	**3**
$h'(0)$	0.7906709	0.778604	0.754471	0.730339
$-k'(0)$	0.236140	0.233642	0.228646	0.223649

Table 2. Stress on the surface for different values of the velocity slip parameter and ferromagnetic interaction number.

is present. In situations where the axis of rotation is not parallel to the gravitational vector, such as those found in space or on Earth, this problem is significant. However, controlling the ferrofluid flow in a zero-gravity environment is possible when a magnetic dipole is there. The following are the primary conclusions of the current investigation:

- The draining speed in the x direction, the induced speed in the y direction, the radial velocity and the axial velocity all rise as the velocity slip parameter is increased. On the other hand, the local heat and mass transport rates are increased by this parameter.
- Increasing the velocity slip parameter and thermal slip parameter can cause the temperature to drop and the concentration of ferrofluid to increase. The heat and mass transfer rates in the flow are decreased by the thermal slip parameter.
- The concentration is lowered by raising the thermophoresis and Brownian motion parameters.
- The thermophoresis parameter increases the mass transfer rate while decreasing the heat transfer rate, and the Brownian motion parameter decreases the mass transfer rate.
- Due to reduced solubility, heat source parameters can decrease concentration while increasing the temperature in the ferrofluid film.
- The findings and understanding gained from this work could be used in many industrial processes, such as coating, lubrication and heat transfer, as well as a variety of medical domains such as targeted medicine therapy and delivery, tissue engineering, etc.

Declaration of interests. The authors report no conflict of interest.

Author ORCIDs.
Anupam Bhandari https://orcid.org/0000-0002-2881-0078;
K.P.S. Parmar https://orcid.org/0000-0001-9165-1543.

References

ACHARYA, N. 2021 Spectral quasi linearization simulation on the radiative nanofluid spraying over a permeable inclined spinning disk considering the existence of heat source/sink. *Appl. Maths Comput.* **411**, 126547.

ALQARNI, A.A., ALVEROĞLU, B., GRIFFITHS, P.T. & GARRETT, S.J. 2019 The instability of non-Newtonian boundary-layer flows over rough rotating disks. *J. Non-Newtonian Fluid Mech.* **273**, 104174.

ANDERSSON, H.I. & VALNES, O.A. 1998 Flow of a heated ferrofluid over a stretching sheet in the presence of a magnetic dipole. *Acta Mech.* **128** (1–2), 39–47.

ARIAS, F.J. 2021 Ferrofluid moving thin films for active flow control. *Chin. J. Aeronaut.* **34** (5), 115–119.

https://doi.org/10.1017/jfm.2024.118 Published online by Cambridge University Press

BACRI, J.C., PERZYNSKI, R., SHLIOMIS, M.I. & BURDE, G.I. 1995 Negative-viscosity effect in a magnetic fluid. *Phys. Rev. Lett.* **75** (11), 2128–2131.

BENTON, E.R. 1966 On the flow due to a rotating disk. *J. Fluid Mech.* **24** (4), 781–800.

BHANDARI, A. 2022 Effect of the diameter of magnetic core and surfactant thickness on the viscosity of ferrofluid. *J. Magn. Magn. Mater.* **548**, 168975.

BHANDARI, A. 2023 Theoretical development in the viscosity of ferrofluid. *J. Tribol.* **145** (5), 050801.

BHANDARI, A. & PARMAR, K.P.S. 2023 Influence of magnetic dipole on ferrohydrodynamic thin film flow over an inclined spinning surface. *Phys. Fluids* **35** (2), 22008.

BLŪMS, E., CEBERS, A.O. & MAĬOROV, M.M. 1997 *Magnetic Fluids*. Walter de Gruyter.

BRYANT, R., WOMELDORF, C., JOHNSSON, E. & OHLEMILLER, T. 2003 Radiative heat flux measurement uncertainty. *Fire Mater.* **27** (5), 209–222.

CHAMKHA, A.J., RASHAD, A.M., REDDY, C.R. & MURTHY, P.V.S.N. 2014 Effect of suction/injection on free convection along a vertical plate in a nanofluid saturated non-Darcy porous medium with internal heat generation. *Indian J. Pure Appl. Maths* **45** (3), 321–342.

CHATTOPADHYAY, S., MUKHOPADHYAY, A. & BARUA, A. 2019 A review on hydrodynamical stability of thin film flowing along an inclined plane. *J. Math. Sci. Model.* **2** (2), 133–142.

COCHRAN, W.G. 1934 The flow due to a rotating disc. *Math. Proc. Camb. Phil. Soc.* **30** (3), 365–375.

CONROY, D.T. & MATAR, O.K. 2015 Thin viscous ferrofluid film in a magnetic field. *Phys. Fluids* **27** (9), 92102.

COWLEY, M.D. 1989 Ferrohydrodynamics. By R. E. Rosensweig. Cambridge University Press, 1985. 344 pp. £45. *J. Fluid Mech.* **200**, 597–599.

DAWAR, A., WAKIF, A., THUMMA, T. & SHAH, N.A. 2022 Towards a new MHD non-homogeneous convective nanofluid flow model for simulating a rotating inclined thin layer of sodium alginate-based Iron oxide exposed to incident solar energy. *Intl Commun. Heat Mass Transfer* **130**, 105800.

FINLAYSON, B.A. 1970 Convective instability of ferromagnetic fluids. *J. Fluid Mech.* **40** (4), 753–767.

GANGADHAR, B.R., KEZIYA, K. & KUMAR, K. 2018 Effect of thermal radiation on heat transfer of ferrofluid over a stretching cylinder with convective heating. *Intl J. Engng Technol.* **7** (4.10), 261.

GOMATHY, B.R. & KUMAR, G. 2023 Variable thermal conductivity and viscosity effects on thin film flow over an unsteady porous stretching sheet. *Spec. Top. Rev. Porous Media Intl J.* **14** (2), 77–94.

GOVINDASAMY, G. & BANGALORE, R.K. 2023 Heat and mass transfer in thin film flow of Casson nanofluid over an unsteady stretching sheet. *Proc. Inst. Mech. Engrs* E *J. Process. Mech. Engng*. **0** (0). doi:10.1177/09544089221150727.

GUL, T., ALTAF KHAN, M., KHAN, A. & SHUAIB, M. 2018 Fractional-order three-dimensional thin-film nanofluid flow on an inclined rotating disk. *Eur. Phys. J. Plus* **133** (12), 500.

HU, B. & KIEWEG, S.L. 2012 The effect of surface tension on the gravity-driven thin film flow of Newtonian and power-law fluids. *Comput. Fluids* **64**, 83–90.

KIM, H., BANKOFF, S.G. & MIKSIS, M.J. 1992 The effect of an electrostatic field on film flow down an inclined plane. *Phys. Fluids* A *Fluid Dyn.* **4** (10), 2117–2130.

KOLE, M. & KHANDEKAR, S. 2021 Engineering applications of ferrofluids: a review. *J. Magn. Magn. Mater.* **537**, 168222.

MAHANTHESH, B. 2021 Flow and heat transport of nanomaterial with quadratic radiative heat flux and aggregation kinematics of nanoparticles. *Intl Commun. Heat Mass Transfer* **127**, 105521.

MICHAELIDES, E.E. 2015 Brownian movement and thermophoresis of nanoparticles in liquids. *Intl J. Heat Mass Transfer* **81**, 179–187.

MIKLAVČIČ, M. & WANG, C.Y. 2004 The flow due to a rough rotating disk. *Z. Angew. Math. Phys.* **55** (2), 235–246.

MOTSA, S.S., RAMREDDY, C. & VENKATA RAO, C. 2017 Non-similarity solution for Soret effect on natural convection over the vertical frustum of a cone in a nanofluid using new bivariate pseudo-spectral local linearisation method. *Appl. Math. Comput.* **314**, 439–455.

MUSTAFA, M. 2017 MHD nanofluid flow over a rotating disk with partial slip effects: Buongiorno model. *Intl J. Heat Mass Transfer* **108**, 1910–1916.

NAIR, S.S., RAJESH, S., ABRAHAM, V.S. & ANANTHARAMAN, M.R. 2011 Ferrofluid thin films as optical gaussmeters proposed for field and magnetic moment sensing. *Bull. Mater. Sci.* **34** (2), 245–249.

NEURINGER, J.L. 1966 Some viscous flows of a saturated ferro-fluid under the combined influence of thermal and magnetic field gradients. *Intl J. Non-Linear. Mech.* **1** (2), 123–137.

NEURINGER, J.L. & ROSENSWEIG, R.E. 1964 Ferrohydrodynamics. *Phys. Fluids* **7** (12), 1927–1937.

NICHOLSON, J.M.P., POWER, H., TAMMISOLA, O., HIBBERD, S. & KAY, E.D. 2019 Fluid dynamics of the slip boundary condition for isothermal rimming flow with moderate inertial effects. *Phys. Fluids* **31** (3), 33602.

https://doi.org/10.1017/jfm.2024.118 Published online by Cambridge University Press

OEHLSEN, O., CERVANTES-RAMÍREZ, S.I., CERVANTES-AVILÉS, P. & MEDINA-VELO, I.A. 2022 Approaches on ferrofluid synthesis and applications: current status and future perspectives. *ACS Omega* **7** (4), 3134–3150.

ROSENSWEIG, R.E. 1985 *Ferrohydrodynamics*. Cambridge University Press.

SAJID, M., AWAIS, M., NADEEM, S. & HAYAT, T. 2008 The influence of slip condition on thin film flow of a fourth grade fluid by the homotopy analysis method. *Comput. Maths Applics.* **56** (8), 2019–2026.

SHAH, Z., ULLAH, A., BONYAH, E., AYAZ, M., ISLAM, S. & KHAN, I. 2019 Hall effect on Titania nanofluids thin film flow and radiative thermal behavior with different base fluids on an inclined rotating surface. *AIP Adv.* **9** (5), 55113.

SHEIKHOLESLAMI, M., HATAMI, M. & GANJI, D.D. 2015 Numerical investigation of nanofluid spraying on an inclined rotating disk for cooling process. *J. Mol. Liq.* **211**, 577–583.

SRIVASTAV, A. & RAMREDDY, C. 2023*a* Case-wise study of thermal radiation in dilatant and pseudoplastic fluid flows: a detailed numerical approach. *Iran. J. Sci. Technol. Trans. Mech. Engng*. https://doi.org/10.1007/s40997-023-00665-7.

SRIVASTAV, A. & RAMREDDY, C. 2023*b* Numerical estimations in a power-law fluid flow with thermal radiation: a complete case study. *Radiat. Eff. Defects Solids* **178** (3–4), 429–441.

STEWARD, F.R. & CANNON, P. 1971 The calculation of radiative heat flux in a cylindrical furnace using the Monte Carlo method. *Intl J. Heat Mass Transfer* **14** (2), 245–262.

THUMMA, T., PYARI, D.R., ONTELA, S., AL-MDALLAL, Q.M. & JARAD, F. 2023 Heat transfer analysis of magnetized Cu-Ag-H2O hybrid nanofluid radiative flow over a spinning disk when the exponential heat source and Hall current are substantial: optimization and sensitivity analysis. *Case Stud. Therm. Engng* **50**, 103448.

TURKYILMAZOGLU, M. 2010 The MHD boundary layer flow due to a rough rotating disk. *Z. Angew. Math. Mech.* **90** (1), 72–82.

UMMEDA, P. & ONTELA, S. 2023 Mixed convective thermally radiative viscoelastic hybrid nanofluid flow in a vertical channel: entropy generation analysis. *Mod. Phys. Lett.* B **38** (04), 2350264.

WANG, C.Y. 2007 Condensation film on an inclined rotating disk. *Appl. Math. Model.* **31** (8), 1582–1593.

WANG, R., *et al*. 2021 A review on slip boundary conditions at the nanoscale: recent development and applications. *Beilstein J. Nanotechnol.* **12**, 1237–1251.

YILBAS, B.S., *et al*. 2022 Ferro-fluid droplet impact on hydrophobic surface under magnetic influence. *Surf. Interfaces* **29**, 101731.

ZABLOTSKY, D., MEZULIS, A. & BLUMS, E. 2009 Surface cooling based on the thermomagnetic convection: numerical simulation and experiment. *Intl J. Heat Mass Transfer* **52** (23–24), 5302–5308.

ZEBIB, A. 1996 Thermal convection in a magnetic fluid. *J. Fluid Mech.* **321**, 121–136.

ZEESHAN, A., RASHEED, H.U., KHAN, W., KHAN, I., ALSHAMMARI, N. & HAMADNEH, N. 2022 Numerical computation of 3D Brownian motion of thin film nanofluid flow of convective heat transfer over a stretchable rotating surface. *Sci. Rep.* **12** (1), 2708.

https://doi.org/10.1017/jfm.2024.118 Published online by Cambridge University Press